Electronic Supplementary Material (ESI) for ChemComm.

Supporting information

for

A superior zinc-air battery performance achieved by CoO/Fe_3O_4 heterostructured nanosheets

Xue Long[a,b#], Wei Tang[b#], Chunsheng Li[c,d], Zhiyong Ma[e], Kai Liu[e], Yi Li[e], Yazhou Chen[a*], Yan Sun[c,d*], Zehui Yang[b] and Fang Luo[a*]

Experimental section

Chemicals: Cobalt (II) nitrate hexahydrate ($Co(NO_3)_2 \cdot 6H_2O$, purity≥99%), Iron (III) nitrate nonahydrate ($Fe(NO_3)_3 \cdot 9H_2O$, purity≥99%) and Iridium (IV) oxide (IrO_2, purity≥99%) were purchased from Aladdin Industrial Corporation. Hexamethylene tetramine (HMTA, purity≥99%) and commercial Pt/C (20 wt.% Pt) were obtained from Sinopharm Chemical Reagent Co. Ltd. Nafion solution (5 wt.%) was purchased from Alfa Aesar. The above-mentioned chemicals and isopropanol, anhydrous ethanol and other gas test reagents were of analytical reagent-grade quality and used directly without additional purification. The deionized water (resistivity≥18.25Ω) used in this work was obtained from ULUPURE system.

Catalyst synthesis: Typically, 1.50 mM $Co(NO_3)_2 \cdot 6H_2O$, 1.60 mM $Fe(NO_3)_3 \cdot 9H_2O$ and 0.85g HMTA were added to the 70mL mixed solution of ethylene glycol and water with a volume ratio of 1 : 2, and then ultrasonically dissolved for 30 minutes to obtain a brown precursor solution. The above solution was transferred into a 100 mL Teflon-lined stainless-steel autoclave and placed in the treated nickel foam which pretreated by hydrochloric acid, anhydrous ethanol and deionized water, followed by the solvothermal process for 10 h at 100 °C. Afterward, the modified NF was collected and washed with deionized water and ethanol, and dried at 65°C for 10 hours in vacuum oven. Due to the surface modification of the CoFe LDH precursor, the NF exhibits orange, which is expressed as CoFe LDH@NF. Subsequently, The CoFe LDH@NF was annealed at 300°C at a heating rate of 2°C/min for 2 hours while 10%NH_3/Ar mixture was introduced. The modified NF become black and is denoted

as CoO/Fe_3O_4 NS@NF. For the synthesis of CoO NS@NF and Fe_3O_4 NS@NF, the process was essentially the same as that of CoO/Fe_3O_4 NS@NF, except that only the corresponding metal salts was introduced during the reparation process of precursor solution.

Material Characterization: The crystal structure and physical phases of the as-prepared electrocatalysts were checked by X-ray diffraction spectroscopy (XRD, D8 Advance) whit Cu Kα radiation in the range of 5-90°. Field emission scanning electron microscope (FE-SEM, FEI, SU8010) and Transmission electron microscopy (TEM, FEI Talos F200x G2) were applied to observe morphologies and microstructures. The specific surface areas and pore size with N_2 adsorption-desorption isotherms were measured by Brunauer-Emmett-Teller (BET, ASAP2460) and Barrett-Joyner-Halenda (BJH) method, respectively. The surface chemical states and electronic structure were determined by X-ray photoelectron spectroscopy (XPS, ESCALAB 250Xi) using non-monochromatized Al-Kα Xray as the excitation source. The correction of recorded binding energy is carried out by referring to the C1s at 284.6 eV, and the Shirley background and XPSPEAK41 software were used for peak fitting. Atomic force microscopy (AFM, FM-Nanoview 1000) was adopted to determine thickness of nanosheets.

Electrochemical Measurement: The OER performance electrochemical measurements of as-prepared electrocatalysts were performed using a Gamry electrochemical workstation in a typical three-electrode configuration at room temperature. The NF modified by active catalyst (denoted as CoO/Fe_3O_4 NS@NF,

Fe_3O_4 NS@NF and CoO NS@NF) were directly used as working electrodes and ensures that the exposed area is 1 * 1cm in the electrolyte; while graphite rod and Hg/HgO electrode (Filled with saturated 1M KOH) serving as the counter electrode and reference electrode, respectively. All of the measured potentials were iR compensated based on the Nernst function with the following equation: $E_{vs\ RHE} = E_{vs\ Hg/HgO} + E_{Hg/HgO} + 0.059*pH$ (pH=14), converted to reversible hydrogen electrode (V vs. RHE). The current density was calculated by the geometric area of the catalyst-loaded NF substrate. Cyclic voltammetry (CV) was carried out at scan rate of 50 mV s^{-1} from 0 to 1.2 (V vs. RHE) to achieve surface activation, stabilized electrode was obtained. Afterward, The OER electrocatalytic activity was evaluated by Linear sweep voltammetry (LSV) at room temperature with scan rate of 5 mV s^{-1}. Electrochemical impedance spectroscopy (EIS) was carried out at the potential corresponding to 10 mA cm^{-2} from 0.1 Hz to 100000 Hz with an amplitude of 10 mV, while operando EIS was obtained by varying the applied potential from 1.026 to 1.676 (V vs. RHE). To estimate the double-layer capacitance (C_{dl}), CV curves were carried out at different scan rates ranging from 10 mV s^{-1} to 100 mV s^{-1} at non-faradaic potential window to demonstrate the current charging and discharging. For the electrocatalysts stability evaluation, CV measurement was performed at scan rate of 100 mV s^{-1} with potential cycling from 1.4 to 1.7 (V vs. RHE) and the LSV curve after 5000 cycles was recorded. The Chronoamperometry method was performed using a voltage corresponding to a current density of 100 m A cm^{-2} without IR compensation.

ORR performance measurements were investigated using a CHI electrochemical station (model 760e) in a standard three electrode system. The rotating disk electrode (RDE, working area: 0.1256 cm^2) loaded with active catalyst, graphite rod and Hg/HgO electrode served as the working electrode, counter electrode and reference electrode, respectively. The active catalysts were obtained from the as-prepared modified NF. Before the measurement, the 1M KOH electrolyte was bubbled with O_2 for 30 min and the flow was continuously introduced to ensure O_2 saturation during the subsequent electrochemical measurement. The catalyst ink was prepared by mixing 0.2 mg active catalysts with 1 mL mixture solution containing 800 μL deionized water, 180 μL isopropanol and 20 μL Nafion (5 wt.%) and then undergo ultrasonic dispersion to form homogeneous ink, which was dropped on the RDE with mass loading of 0.382 mg cm^{-2}. For comparison, the Pt/C (20 wt.%) catalyst ink was prepared. LSV was scanned from 1.0 to 0.2 (V vs. RHE) with a scan rate of 5 mV s^{-1} at the rotating speed of 1600 rpm. Similarly, CV and CA measurement were adopted to estimate the ORR stability.

The electron transfer number (n) of ORR electrocatalysis process were calculated by the Koutecky-Levich (K-L) equation:

$$\frac{1}{i}=\frac{1}{i_L}+\frac{1}{i_\kappa}=\frac{1}{i_L}+\frac{1}{0.62nFC_0(D_0)^{2/3}v^{-1/6}\omega^{1/2}}$$

Where *i,* i_L and i_k represent the limiting current density, the diffusion-limiting current density, and the kinetic current density, respectively. F is the Faraday constant (96485 C mol^{-1}), C_o is the bulk concentration of O_2, D_o represent the diffusion coefficient of O_2 and υ is the kinematic viscosity of the solution. ω indicates the

rotation rate of the RDE ($\omega=2\pi N$，N refers to the linear rotation speed). Difference LSV polarization curves were recorded at a scan rate of 5 mV s^{-1} with various electrode rotation rate (ω=400, 600, 800, 1200, 1600 and 2400 rpm) and then n was calculated in the range of 0.35-0.60 (V vs. RHE) by using the K-L equation above.

Fabrication and measurement of Zinc air batteries: The self-assembled ZAB consists of electrolyte, metal anode (a polished Zn plate), air cathode and the current collectors (NF). In the air electrode, a piece of NF on the air-facing side as the current collector, the as-prepared material was directly used as catalyst layer on the electrolyte-facing side without any binders and a gas diffusion layer (GDL) in the middle, which allows the surrounding O_2 from ambient air to reach the catalyst layer. 6M KOH+0.2M $Zn(Ac)_2$ and Polyvinyl acetate (PVA-KOH) gel were used as electrolyte in liquid and solid-state ZAB, respectively. For the preparation of solid-state electrolyte, 1 g PVA were add into 10 mL deionized water and stirred at 90°C for 30 min to form a transparent mucus, which was added dropwise to 18M KOH solution containing 0.2M $Zn(Ac)_2$, and stirred continuously for 30 min. Then, the mixed solution was frozen and refrigerated to form a polymer film. Finally, it was immersed in 18M KOH+0.2M $Zn(Ac)_2$ for a whole night, the solid electrolyte was obtained. To prepare Pt/C-IrO_2 catalyst layer, 1 mL homogeneous catalyst ink containing 1 mg Pt/C and 1 mg IrO_2 was sprayed on carbon cloth (1*1 cm) that construct air-electrode of ZAB. The electrochemical measurements of batteries were performed on VMP3 and Gamry electrochemical workstation at room temperature. The open-circuit potential tests were carried out by Gamry electrochemical

workstation. In Vmp3 system, the polarization curves were recorded by LSV with discharge speed of 10 mV s^{-1} and charge speed of 1 mV s^{-1} and the power density is obtained by the corresponding discharge polarization curve. The galvanostatic charge/discharge tests were measured at the current density of 5 mA cm^{-2} with 20 min per cycle (10 min charge and 10 min discharge). The specific capacity (mAh g_{Zn}^{-1}) was calculated by the corresponding current densities and discharge time using the amount of consumed Zn during the discharge test at 5 mA cm^{-2}.

Table S1 Quantitative analysis of Co^0/Co^{2+} and Fe^{2+}/Fe^{3+} ratios.

Electrocatalyst	Co^0/Co^{2+}	Fe^{2+}/Fe^{3+}
CoO	1.28	-
Fe_3O_4	-	0.75
CoO/Fe_3O_4	0.98	0.88

Table S2 Comparison of the battery performances of the reported electrocatalysts.

Catalyst	j ($mA \cdot cm^{-2}$)	Power density ($mW \cdot cm^{-2}$)	Time of cycle life tests (h)	Reference
CoO/Fe_3O_4-NS	5	276.2	600	This work
Pt/C-IrO_2	5	133.2	20	This work
Fe_3C/Fe_2O_3@NGN	10	139.8	60	[1]
Co/CoO@FeNC-850	5	132.8	50	[2]
Co-NC@LDH	5	107.8	300	[3]
Co_3O_4@NiFe-LDH	15	127.4	200	[4]
FeNiS-NBC/C	5	133.0	130	[5]
P-CoNi@NSCs	5	87.9	620	[6]
Ni–Co/NFC	20	138.0	200	[7]
TMB@NiNC	10	107.0	230	[8]
Ni_3S_4@CoSx-NF	5	143.0	667	[9]
$Sr_2Fe_{1.5}Mo_{0.5}O_{6-\delta}$	10	137.0	300	[10]
MnOx-FeNi-LDH/NF	10	120	110	[11]
Co-NC@Nb-TiOx	10	123.46	225	[12]

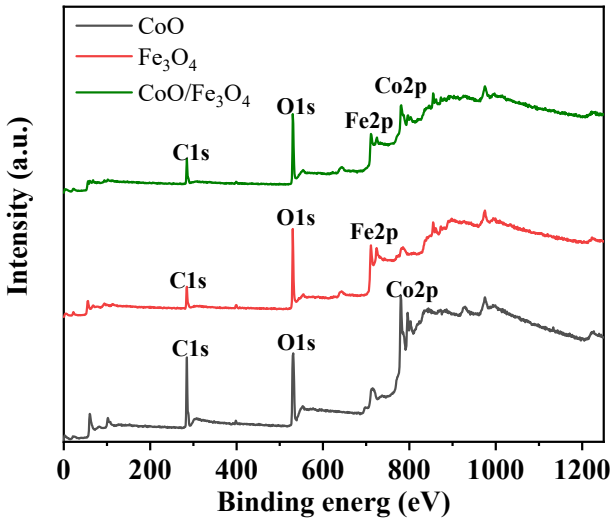

Figure S1 XPS survey scan of CoO-NS, Fe_3O_4-NS and CoO/Fe_3O_4-NS electrocatalyst.

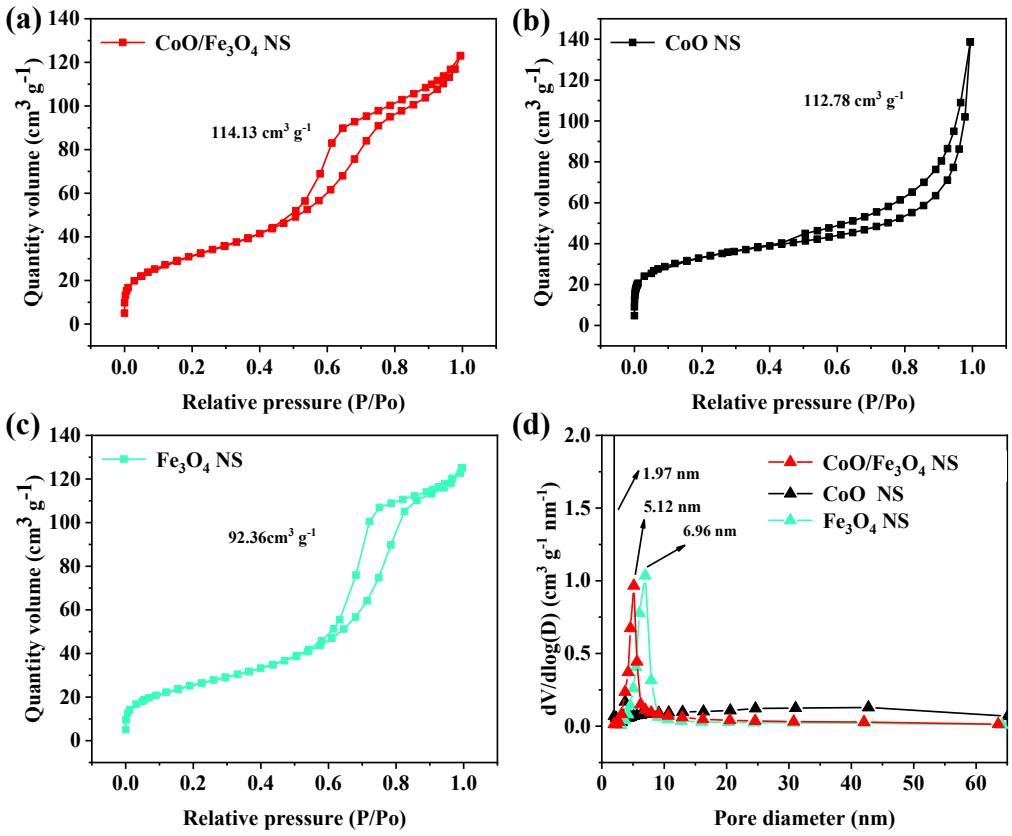

Figure S2 N_2 isothermal curves and pore size distribution of CoO-NS, Fe_3O_4-NS and CoO/Fe_3O_4-NS electrocatalyst.

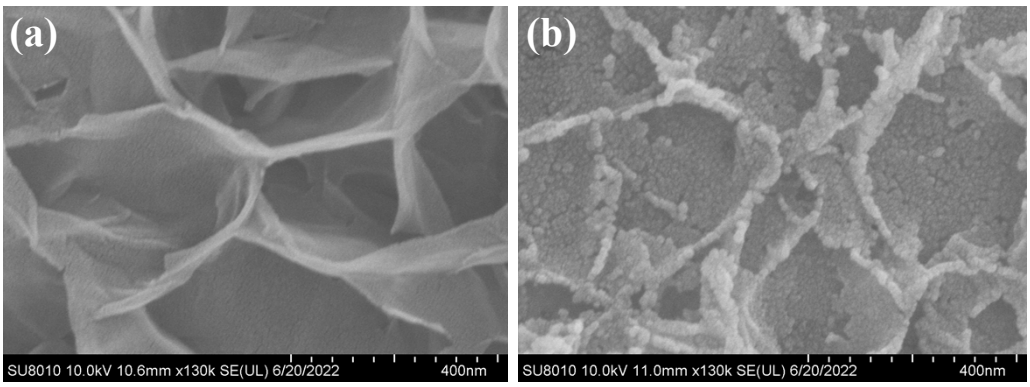

Figure S3 SEM images of CoO-NS (a) and Fe_3O_4-NS (b) electrocatalysts.

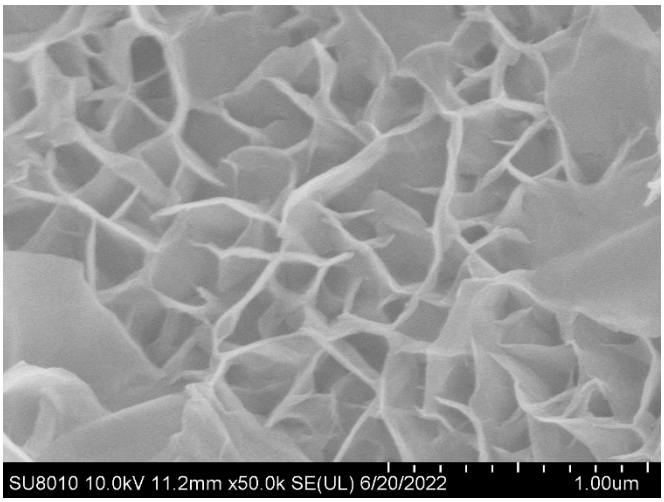

Figure S4 SEM image of CoFe-LDH electrocatalyst.

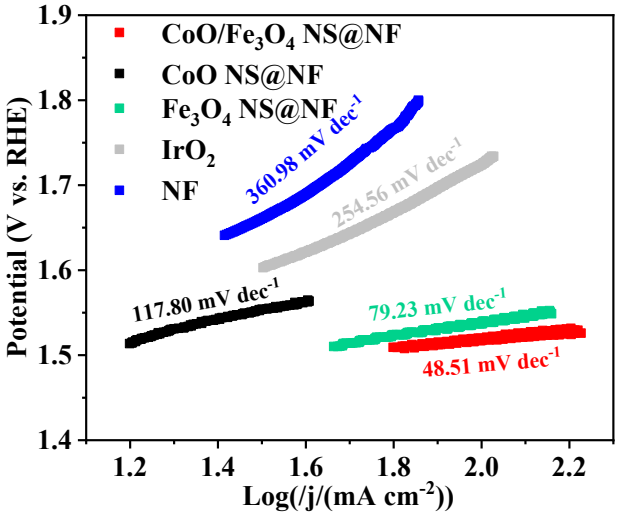

Figure S5 Tafel slopes of various electrocatalysts in OER catalysis.

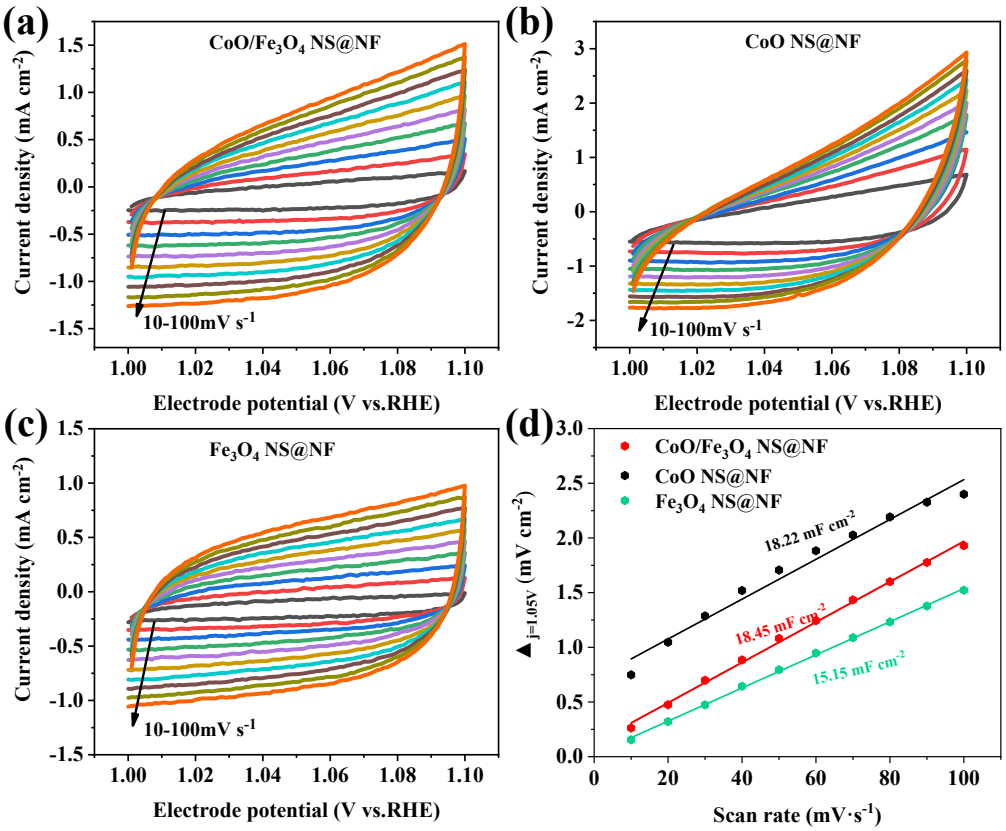

Figure S6 Cyclic voltammetry curves of CoO/Fe3O4-NS, CoO-NS, Fe3O4-NS and double layer capacitances.

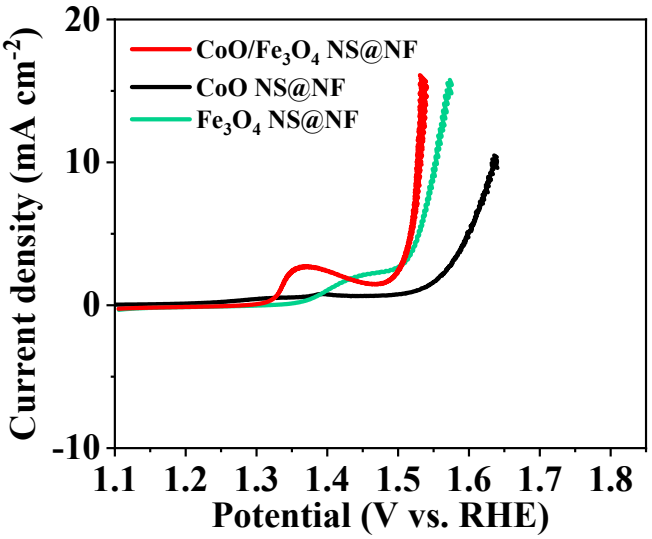

Figure S7 Specific activities of CoO-NS, Fe_3O_4-NS and CoO/Fe_3O_4-NS electrocatalysts.

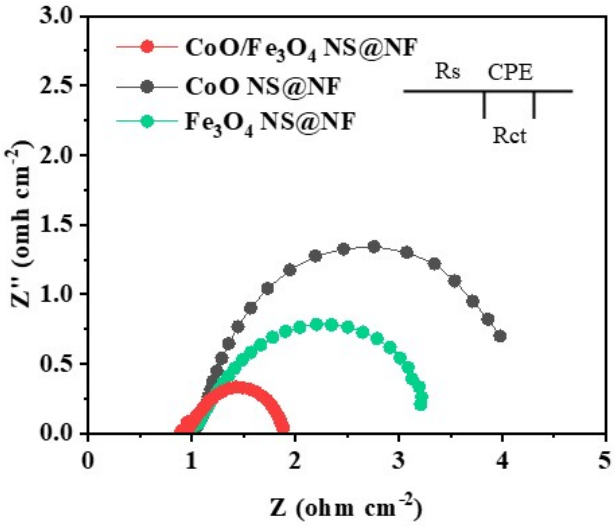

Figure S8 Electrochemical impedance spectroscopies of CoO-NS, Fe_3O_4-NS and CoO/Fe_3O_4-NS electrocatalysts.

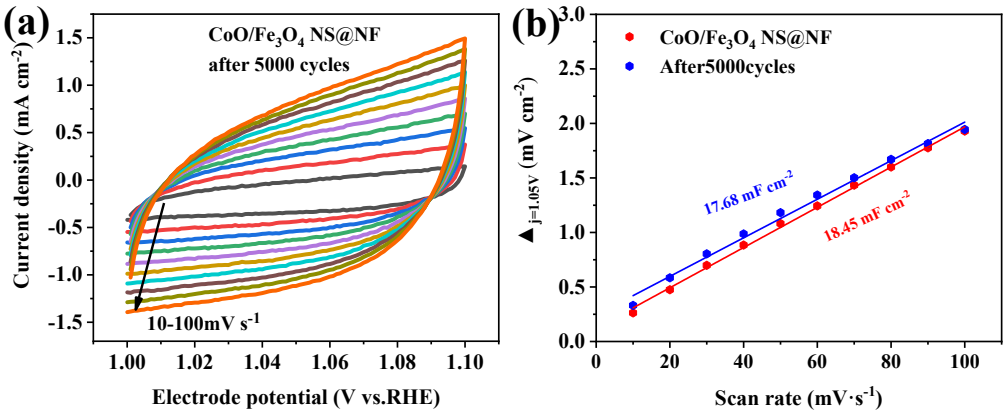

Figure S9 Cyclic voltammetry curve and double layer capacitances of CoO/Fe_3O_4-NS after 5000 cycles.

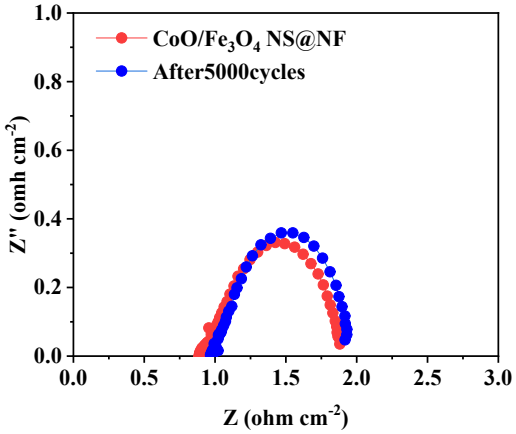

Figure S10 Electrochemical impedance spectroscopies of CoO/Fe_3O_4-NS after 5000 cycles.

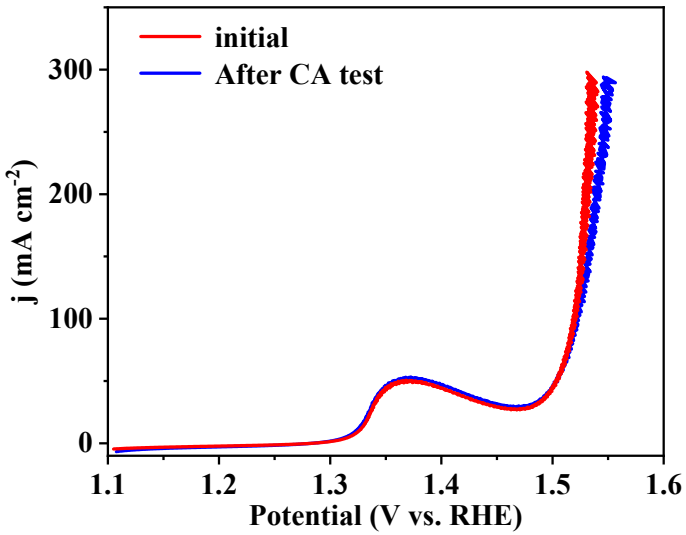

Figure S11 OER performance of CoO/Fe_3O_4-NS before and after CA test.

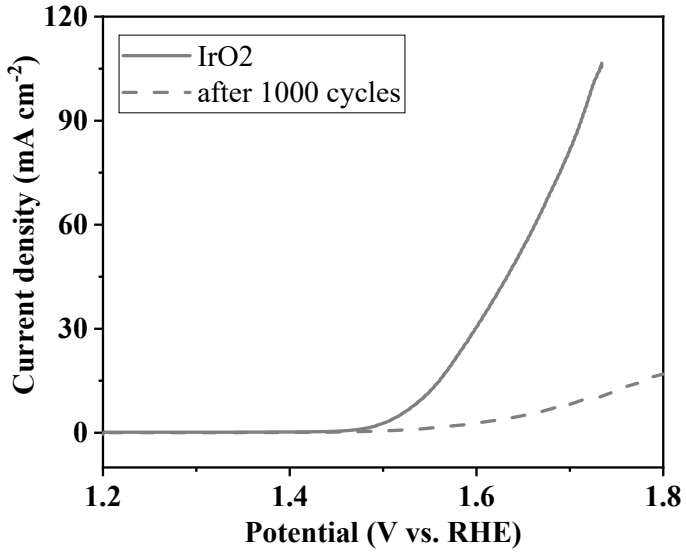

Figure S12 OER performance of commercial IrO_2 before and after 1000 cycles.

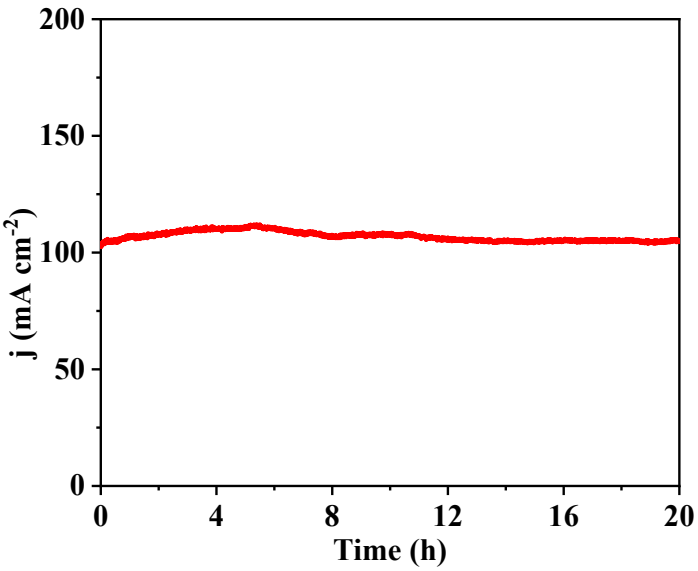

Figure S13 i-t test of CoO/Fe_3O_4-NS during 20 h.

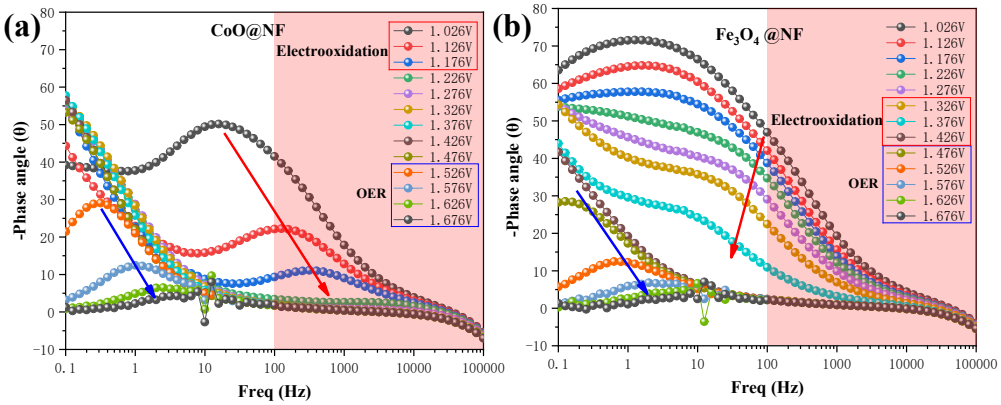

Figure S14 Bode plots of CoO-NS and Fe_3O_4-NS in OER catalysis.

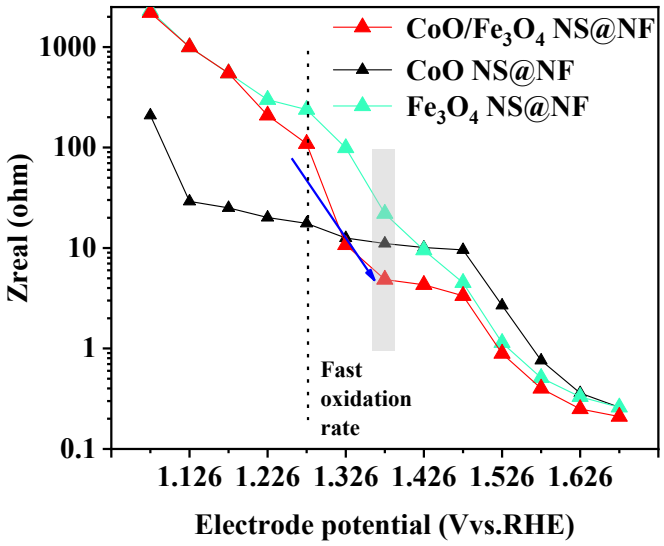

Figure S15 R_{ct} values of CoO-NS, Fe_3O_4-NS and CoO/Fe_3O_4-NS at various potentials.

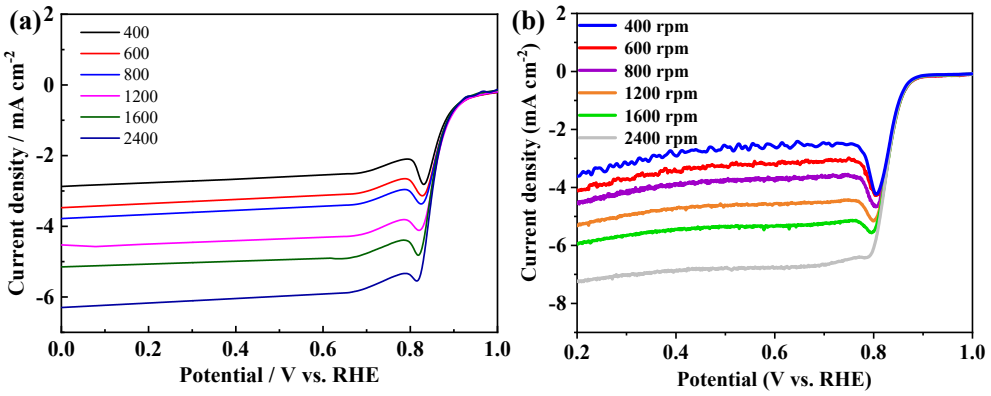

Figure S16 ORR curves of CoO/Fe_3O_4-NS and commercial Pt/C at various ration speeds.

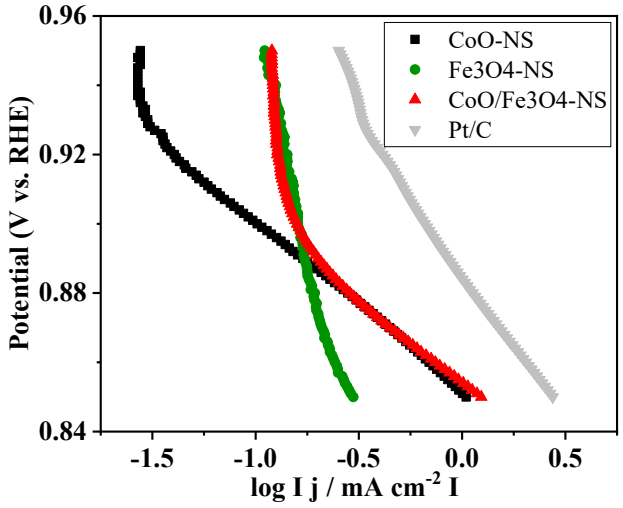

Figure S17 Tafel slopes of CoO-NS, Fe_3O_4-NS, Pt/C and CoO/Fe_3O_4-NS.

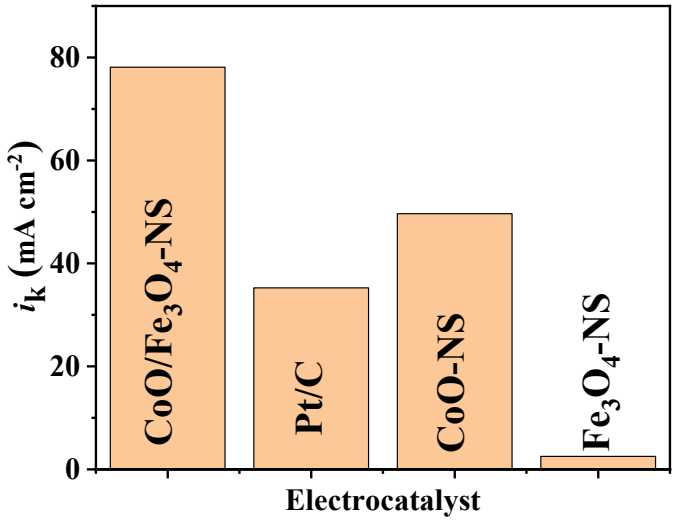

Figure S18 Kinetic current density of CoO-NS, Fe_3O_4-NS, Pt/C and CoO/Fe_3O_4-NS at 0.8 V vs. RHE.

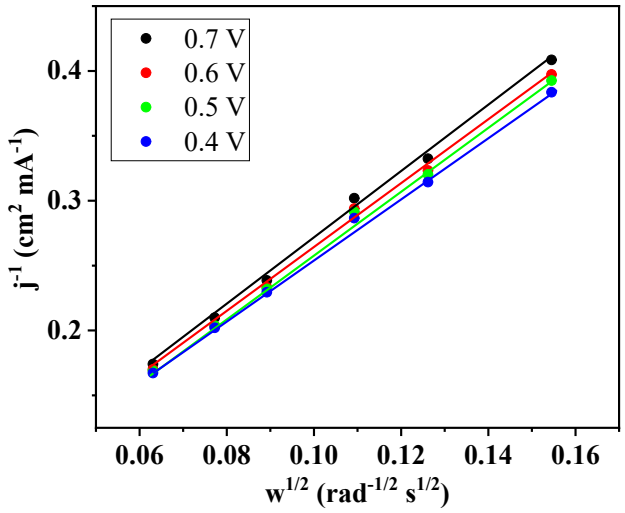

Figure S19 K-L equations of commercial Pt/C at various potentials.

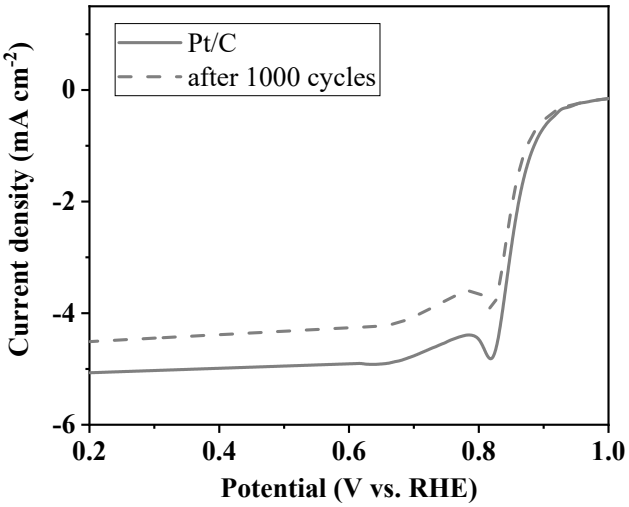

Figure S20 ORR performance of commercial Pt/C before and after 1000 cycles.

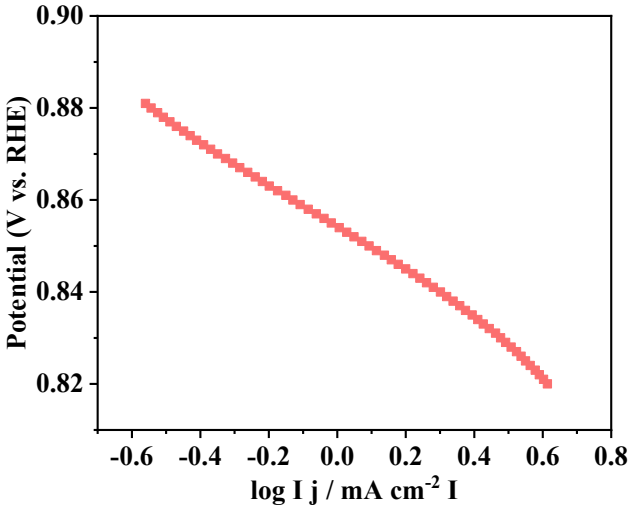

Figure S21 Tafel slope of CoO/Fe_3O_4-NS before and after 1000 cycles.

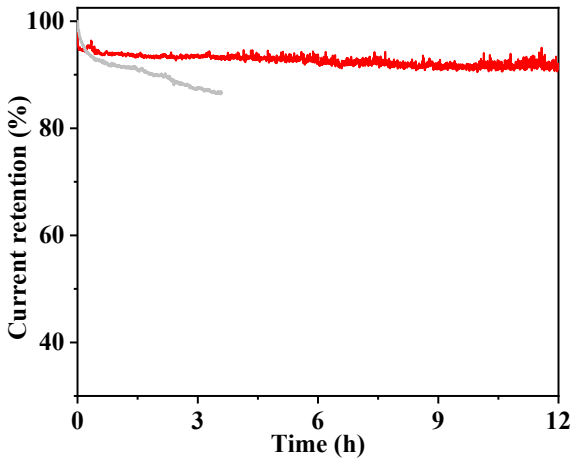

Figure S22 i-t test of CoO/Fe3O4-NS and Pt/C.

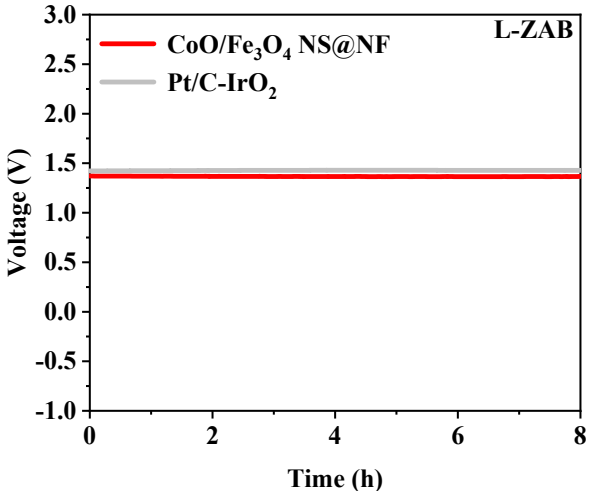

Figure S23 Open circuit voltage test of zinc-air batteries fabricated from CoO/Fe_3O_4-NS and Pt/C-IrO_2.

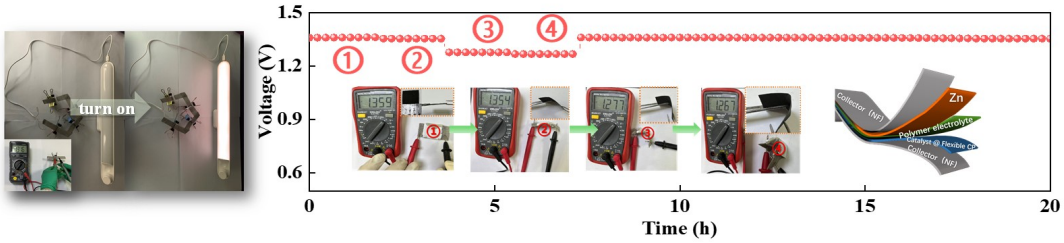

Figure S24 Photo of OCV test of all-solid-state ZAB with different bending angles.

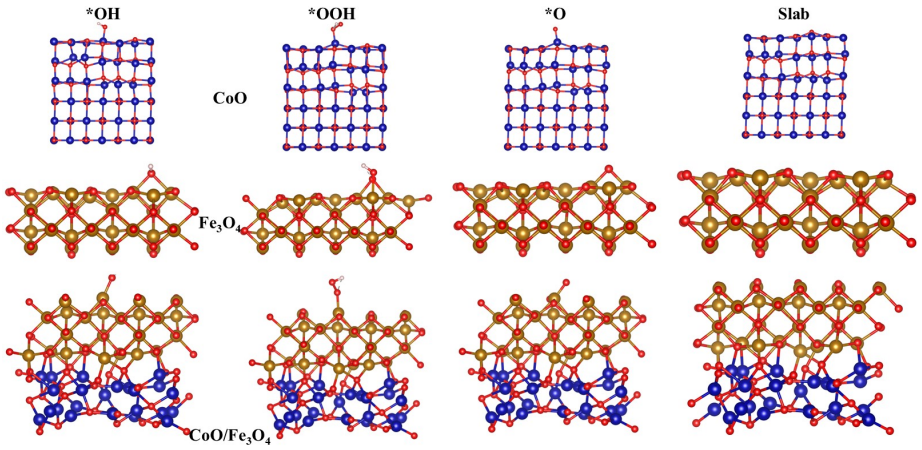

Figure S25 Structures of oxygen intermediates adsorbed on CoO, Fe_3O_4 and CoO/Fe_3O_4.

References

1. Y. H. Tian, L. Xu, J. C. Qian, J. Bao, C. Yan, H. N. Li, H. M. Li and S. Q. Zhang, *Carbon*, 2019, 146, 763-771.
2. Y. Chen, C. Gong, Z. Shi, D. Chen, X. Chen, Q. Zhang, B. Pang, J. Feng, L. Yu and L. Dong, *Journal of Colloid and Interface Science*, 2021, 596, 206-214.
3. D. Chen, X. Chen, Z. Cui, G. Li, B. Han, Q. Zhang, J. Sui, H. Dong, J. Yu, L. Yu and L. Dong, *Chemical Engineering Journal*, 2020, 399.
4. X. L. Guo, X. L. Hu, D. Wu, C. Jing, W. Liu, Z. L. Ren, Q. N. Zhao, X. P. Jiang, C. H. Xu, Y. X. Zhang and N. Hu, *Acs Applied Materials & Interfaces*, 2019, 11, 21506-21514.
5. Y. X. Wang, R. J. Liu, W. D. Chen, W. M. Li, W. Zheng, H. Zhang and Z. Y. Zhang, *Acs Sustainable Chemistry & Engineering*, 2022, 10, 14486-14494.
6. X. H. He, J. Fu, M. Y. Niu, P. F. Liu, Q. Zhang, Z. Y. Bai and L. Yang, *Electrochimica Acta*, 2022, 413.
7. M. H. Wang, S. Ji, H. Wang, V. Linkov, X. Y. Wang and R. F. Wang, *Journal of Power Sources*, 2023, 571.
8. M. Moloudi, A. Noori, M. S. Rahmanifar, Y. Shabangoli, M. F. El-Kady, N. B. Mohamed, R. B. Kaner and M. F. Mousavi, *Advanced Energy Materials*, 2022, DOI: 10.1002/aenm.202203002.
9. M. M. Yin, H. Miao, J. X. Dang, B. Chen, J. Q. Zou, G. M. Chen and H. Li, *Journal of Power Sources*, 2022, 545.
10. J. Zhou, T. Liu, J. Zhang, L. Zhao, W. He and Y. Wang, *Separation and Purification Technology*, 2023, 304.
11. L. Wan, P. C. Wang, Y. Q. Lin and B. G. Wang, *Journal of the Electrochemical Society*, 2019, 166, A3409-A3415.
12. T. T. Wan, H. Y. Wang, L. L. Wu, C. C. Wu, Z. S. Zhang, S. M. Liu, J. Fu and J. D. Li, *Journal of Colloid and Interface Science*, 2023, 651, 27-35.